Catalysis Today 224 (2014) 114–121

Contents lists available at ScienceDirect

Catalysis Today

journal homepage: www.elsevier.com/locate/cattod

Hierarchical nanocomposites of polyaniline nanorods arrays on graphitic carbon nitride sheets with synergistic effect for photocatalysis

Shouwei Zhang[a,b], Lanping Zhao[c], Meiyi Zeng[a], Jiaxing Li[b], Jinzhang Xu[a,*], Xiangke Wang[b,*]

[a] School of Materials Science and Engineering, Hefei University of Technology, Hefei 230031, China
[b] Key Laboratory of Novel Thin Film Solar Cells, Institute of Plasma Physics, Chinese Academy of Sciences, PO Box 1126, 230031 Hefei, China
[c] Education Training Center of Ningxia Electric Power Company, Yinchuan, Ningxia 750011, China

ARTICLE INFO

Article history:
Received 31 July 2013
Received in revised form
22 November 2013
Accepted 2 December 2013
Available online 22 December 2013

Keywords:
Hierarchical structures
g-C_3N_4-PANI
Heterojunction
Charge separation
Photocatalysis

ABSTRACT

Hierarchical nanocomposites of polyaniline (PANI) nanorod arrays on graphitic carbon nitride (g-C_3N_4) sheets (CN-PANI) were successfully synthesized by dilute polymerization under −20 °C. The photocatalytic activities of the CN-PANI composites were evaluated using methylene blue (MB) and methyl orange (MO) as model pollutants. The CN-PANI composites displayed much higher photocatalytic activity than the pure g-C_3N_4 and PANI under visible light irradiation. Meanwhile, the degradation efficiency of MO was higher than that of MB under same irradiation conditions, which was mainly attributed to the difference of adsorption processes. The different adsorption behaviors of MB and MO on composites were due to the fact that they carry different charge, i.e., MO and CN-PANI composites have the opposite charge, leading to the enhanced MO adsorption due to the strong electrostatic forces between them. Conversely, MB had the same charge with PANI, thus resulting in a low adsorption capacity due to the electrostatic repulsion. By careful investigation of the influence parameters, a possible mechanism was proposed, i.e., the synergistic effect of g-C_3N_4 and PANI was responsible for the effective photogenerated charge separation, the large specific surface area and the energy band structure.

Introduction

Organic pollution due to the indiscriminate disposal of wastewater is a worldwide environment concern and is harmful to human health. It is necessary to eliminate organic pollutants from wastewater before its release into the natural environment. For this reason, different methodologies, such as adsorption, oxidation, reduction, and electrochemical reactions, are proposed to remove these pollutants from aqueous solutions [1]. Among these methods, semiconductor photocatalysis as a high-profile method has been widely applied in degradation of organic pollutants [2].

As the most widely used photocatalyst, TiO_2 is a promising material for photocatalytic treatment of pollutants in water due to its peculiarities of chemical inertness, resistance to photocorrosion, low cost, and non-toxicity [3–5]. However, TiO_2 is a wide-band gap semiconductor (3.2 eV for anatase) and could only absorb about 3–5% of sunlight in the ultraviolet region, which greatly limits its practical applications [6]. Therefore, the development of visible-light-driven photocatalysts has become a very important topic of research.

Recently, g-C_3N_4 has attracted much attention in the field of photocatalysis for its non-toxicity and abundance [7,8], which is only made up of carbon and nitrogen, could be used as a metal-free photocatalyst for solar energy conversion, hydrogen production and environmental pollution purification [9]. Moreover, unlike many photocatalysts of sulfide and oxynitride semiconductor, g-C_3N_4 is highly stable with respect to thermal, chemical, and photochemical attack owing to its tri-s-triazine ring structure and high degree of condensation [9]. All these superior properties imply that the g-C_3N_4 should be an ideal candidate material and holds promising potential in photocatalytic fields. However, there are many drawbacks of the g-C_3N_4 for photocatalysis, which include: (1) the high recombination rate of photogenerated charge, (2) an optical band gap of 2.7 eV, namely, the lack of absorption above 460 nm for solar spectra, and (3) the lower specific surface area [10].

To date, continuous attempts have been carried out to improve the photocatalysis efficiency of g-C_3N_4, for example, by chemical doping with metal or nonmetal elements [11–13], designing

* Corresponding authors. Tel.: +86 551 65592788; fax: +86 551 65591310.
E-mail addresses: xujz@lzu.edu.cn (J. Xu), xkwang@ipp.ac.cn (X. Wang).

0920-5861/$ – see front matter © 2013 Elsevier B.V. All rights reserved.
http://dx.doi.org/10.1016/j.cattod.2013.12.008

nanoporous structures [14,15], and coupling with graphene [16,17], etc. The most promising solution is combining g-C_3N_4 with other semiconductors with suitable band gap to extend the absorption range of g-C_3N_4. Meanwhile, heterojunctions might be formed between the g-C_3N_4 and other semiconductors, which provides a potential driving force for the separation of photogenerated charge at the interfaces.

In the last decade, polyaniline (PANI) as photocatalyst has been the most extensively investigated in photocatalytic area, because it is one type of conducting polymer with good stability, corrosion protection, non-toxicity, facile and low cost synthesis [18]. Particularly, PANI has shown great potential due to its high absorption coefficient ($\sim 5 \times 10^4$) in the visible-light range and high mobility of charge carriers [19]. Furthermore, PANI is not only an electron donor but also an excellent hole acceptor after irradiation [20]. Therefore, PANI is usually adopted as an important additive to enhance the charge separation efficiency of the photocatalyst. Recently, more attentions have been focused on the combination of PANI with semiconductor photocatalysts. Zhang et al. [21] and Wang et al. [22] prepared PANI/TiO_2 composites via chemisorptions and in situ oxidative polymerization and then found the as-prepared samples had enhanced photocatalytic activity under natural light. Furthermore, PANI-CdS [23] and PANI-$BiVO_4$ [24] have also been developed and demonstrated efficient photocatalytic activity. Therefore, it is expected that the g-C_3N_4-PANI photocatalyst from the combination of the PANI with g-C_3N_4 should have efficient photocatalytic activity under visible light irradiation.

Herein, we prepared hierarchical composites of PANI nanorods grown on the surface of g-C_3N_4 sheets used as the photocatalyst. The photocatalytic activities of the CN-PANI heterojunction composites were evaluated using methylene blue (MB) and methyl orange (MO) as model pollutants. The possible photocatalytic mechanism was discussed and proposed based on the experimental results.

Experiment section

Materials

Urea (99.3%, Alfa Aesar), aniline monomer (≥99.5%, Sigma-Aldrich), perchloric acid ($HClO_4$), ammonium persulfate ($(NH_4)_2S_2O_8$, (APS)) and ethanol were analytical purity and were from Sinopharm Chemical Reagent Co., Ltd.

Synthesis of g-C3N4

g-C_3N_4 sheets were prepared according to a reported procedure [25]. In detail, 20 g urea (99.3%, Alfa Aesar) was put in a crucible with a cover and heated under static air in muffle furnace (Hefei Branch Crystal Materials Technology Co., Ltd., China) at 550 °C for 4 h with a ramping rate of 2.5 °C/min. The resultant light yellow powder was rinsed with deionized water and dried in a vacuum oven at 60 °C.

Synthesis of CN-PANI nanocomposites

CN-PANI nanocomposites were synthesized by dilute polymerization of g-C_3N_4 and aniline monomer [26]. In a typical procedure, 400 mg (or 200 mg, 600 mg) g-C_3N_4 was added into 160 mL of 1 M $HClO_4$ ethanol solution, and the mixtures were stirred until g-C_3N_4 was fully dispersed. Then 0.05 M aniline monomer (≥99.5%, Sigma-Aldrich) was added into the above solution and stirred for 30 min at −20 °C to form uniform mixtures. The oxidant, $(NH_4)_2S_2O_8$ (APS) (the molar ratio of aniline/APS is 1.5) was dissolved in 40 mL of $HClO_4$ ethanol solution and cooled to −20 °C in refrigerator. The polymerization was performed after rapid addition of the pre-cooled APS solution, and the mixture was stirred for 24 h at −20 °C. Finally, the black green precipitates were filtered and washed with water and ethanol. The samples were dried at 60 °C for 24 h under vacuum, and the 400CN-PANI (200CN-PANI, 600CN-PANI) composites were obtained.

Sample characterization

The crystal structures were analyzed by X-ray powder diffraction (XRD) patterns were recorded in reflection mode (Cu$K\alpha$ radiation, $\lambda = 1.5418$ Å) on a Scintag XDS-2000 diffractometer. Fourier transforms infrared spectroscopy (FT-IR) was carried out on a Bruker EQUINOX55 spectrometer (Nexus) in KBr pellet at room temperature. The morphology and microstructures were observed using a field emission scanning electron microscope (FE-SEM, Sirion200, FEI Corp., Holland) and transmission electron microscopy (TEM, JEM-2011, JEOL, Japan). UV–Vis spectra were recorded on a Shimadzu UV-2550 spectrophotometer equipped with a Labsphere diffuse reflectance accessory. Thermogravimetric (TG) were measured by using a Shimadzu TGA-50 thermogravimetric analyzer from room temperature to 800 °C with heating rate of 10 °C/min and Ar flow rate of 50 mL/min. The N_2 adsorption–desorption isotherms at 77 K were measured using an adsorption instrument (TriStarII, Micromeritics Company, USA) to evaluate their pore structures and surface area. The electrochemical measurements were carried out on a CHI 660D electrochemical workstation (Shanghai Chen Hua Instrument Co., Ltd., China) by using three-electrode cells at room temperature.

Photocatalysis experiment

MB and MO were chosen as model pollutants for the photocatalytic degradation experiments. The photocatalytic activity of the various photocatalysts (25 mg) were examined by monitoring the degradation of an aqueous suspension of 100 mL of 10 mg/L MB/MO in a beaker under a constant stirring condition at 400 rpm/min at room temperature. The visible light source for the photo-irradiation was a 500 W Xe lamp (Beijing Zhongjiaojinyuan Technology Co., Ltd.) with a super cold filter, which provided the visible light region ranging from 400 nm to 700 nm. Prior to irradiation, the photocatalyst was suspended in the solutions with constant stirring under dark conditions for 2 h to ensure that the surface of the catalyst was saturated with MB/MO. During the photocatalysis processes, the samples (3 mL) were periodically withdrawn. The absorption spectra were recorded on a UV–Vis spectrophotometer (UV-2550, Shimadzu) at the maximal absorption wavelength of 663 nm (MB)/464 nm (MO).

Results and discussion

The XRD patterns of PANI, g-C_3N_4, 400CN-PANI composites are shown in Fig. 1. For pure g-C_3N_4, the strong peak located at 27.21 was the typical interplanar stacking peak of conjugated aromatic systems. The other peak at 12.81 belongs to an in-planar structural packing motif. Both peaks were the characteristic peaks commonly found in carbon nitride [27]. As compare to the pure g-C_3N_4, two new broad peaks at 20.12 and 25.26 were found in 400CN-PANI composite, which were the characteristic peaks of PANI [28]. The characteristic peaks of g-C_3N_4 sheets were less pronounced in 400CN-PANI, because the g-C3N4 was cover with PANI. The percentage of PANI in composite was measured by TG and the PANI contents in the 400CN/PANI composite were determined to be ~72%.

The FTIR spectra of g-C_3N_4 and 400CN-PANI composites were shown in Fig. 2. For g-C_3N_4, the bands at 1640.5 cm^{-1}, 1569.1 cm^{-1}, 1462.1 cm^{-1} and 1412.2 cm^{-1} were assigned to typical stretching vibration modes of heptazine-derived repeating

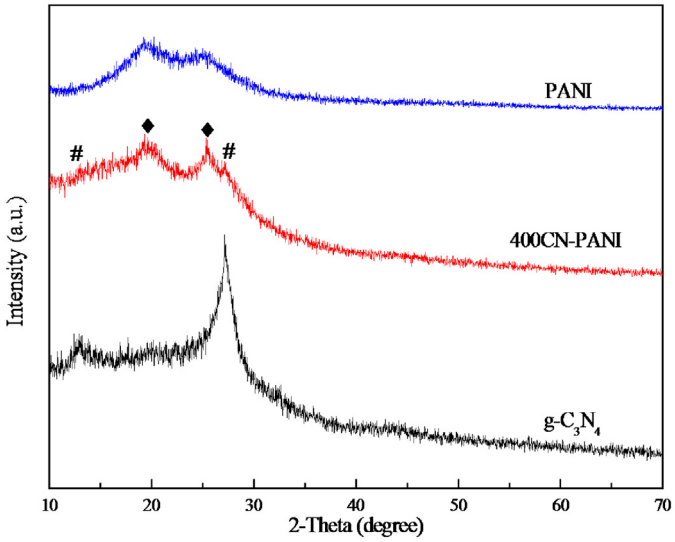

Fig. 1. XRD patterns of PANI, g-C_3N_4 and the 400CN-PANI composite photocatalysts.

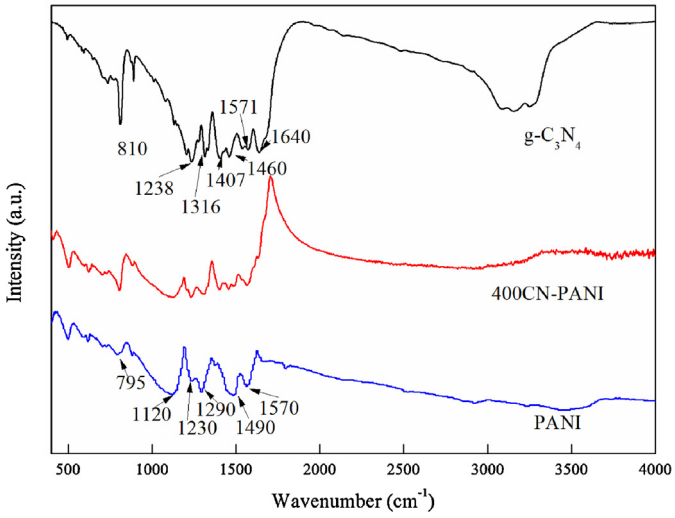

Fig. 2. FTIR spectra of PANI, g-C_3N_4 and the 400CN-PANI composite photocatalysts.

units [29]. The intense band at 812.1 cm^{-1} represented the out-of-plane bending vibration characteristic of heptazine rings. The bands at 1321.8 cm^{-1} and 1243.3 cm^{-1} corresponded to stretching vibration of connected units of C–N(–C)–C (full condensation) or C–NH–C (partial condensation), which was also supported by the stretching vibration modes of the broad weak band at ~3235.9 cm^{-1} for hydrogen-bonding interactions. The broad band at 3000–3700 cm^{-1} belongs to N–H vibration due to partial condensation and the adsorbed water molecules. The absorption peaks at 1570 cm^{-1} (the aromatic C=C stretching of the quinonoid ring), 1490 cm^{-1} (the aromatic C=C stretching of the benzenoid ring), 1290 cm^{-1} (the C–N stretching of the secondary aromatic amine), 1230 cm^{-1} (the C–N^+ stretching), 1120 cm^{-1} (the =N^+–H stretching), and 795 cm^{-1} (the aromatic C–H out-of-plane deformation vibration) are the characteristic peaks of PANI. Compared to g-C_3N_4, the new absorption peaks at 1572 cm^{-1}, 1491 cm^{-1}, 1290 cm^{-1}, 1231 cm^{-1}, 1122 cm^{-1}, and 796 cm^{-1} were shown in 400CN-PANI composite, due to the existence of PANI [30]. All the characteristic peaks of g-C_3N_4 and PANI were observed in the 400CN-PANI composites.

The optical absorption of the g-C_3N_4 and 400CN-PANI composites are shown in Fig. 3. The absorption edge at 460 nm in pure

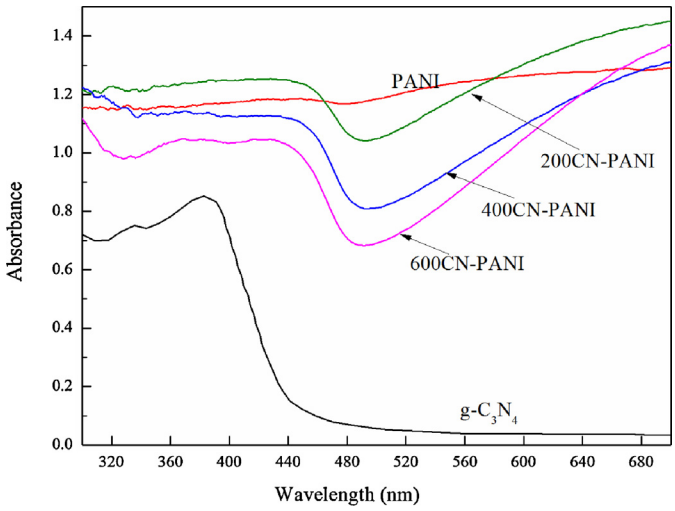

Fig. 3. UV–Vis spectra of PANI, g-C_3N_4 and CN-PANI composite photocatalysts.

g-C_3N_4 could be ascribed to the band gap of g-C_3N_4 (2.7 eV) [31]. The pure PANI sample can not only absorb UV light, but also has strong absorption in visible light and near infrared regions, which can be ascribed to transitions in the PANI molecules [32]. Compared with the pure g-C_3N_4, the composite exhibited stronger absorption in the visible region at wavelengths longer than 400 nm, and the obvious red shift was observed [33]. The UV–Vis spectra results indicated that CN-PANI can be excited to generate more electron–hole pairs under visible light irradiation, and this was expected to enhance the photocatalytic performance.

The N_2 adsorption–desorption isotherms of the g-C_3N_4 and 400CN-PANI composites are shown in Fig. 4. The specific surface area of g-C_3N_4 was only 25.6 m^2/g, and then lead to low adsorption of dye molecules onto it and thereby further results in low photocatalytic activity. The specific surface area of 400CN-PANI was 95.4 m^2/g, which was ~3 times higher than that of g-C_3N_4. This high specific surface area provided more active sites for the adsorption and photocatalytic reaction, enhanced the interfacial reaction process, and improved photocatalysis performance.

The morphologies of g-C_3N_4 and 400CN-PANI composites were observed by SEM and TEM, as shown in Fig. 5. Interestingly, a two dimensional sheet-like structure consisting of winkles can be observed in the g-C_3N_4 sample, which was the analogue of

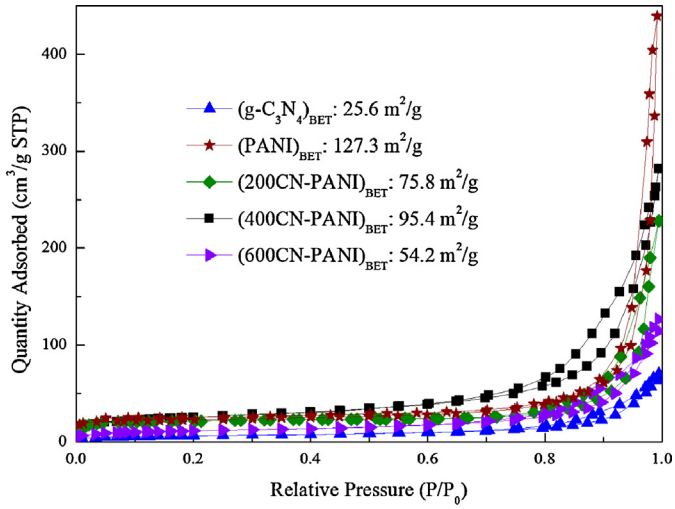

Fig. 4. Nitrogen adsorption–desorption isotherms of g-C_3N_4, PANI and CN-PANI composite photocatalysts.

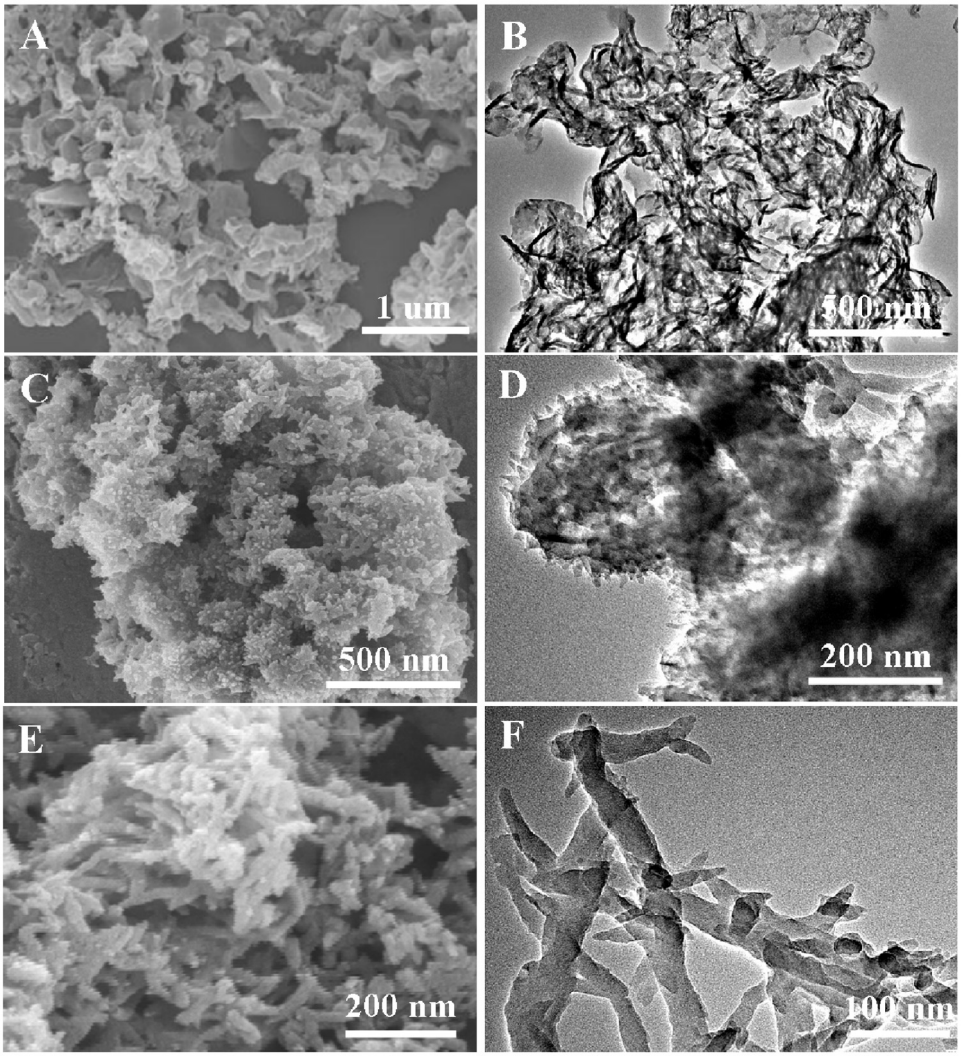

Fig. 5. The SEM (A) and TEM (B) images of g-C_3N_4. The SEM (A) and TEM (B) images of 400CN-PANI composites. The SEM (E) and TEM (F) images of PANI.

crumpled graphene [34] (Fig. 5A and B). It can be seen that g-C_3N_4 nanosheets exhibited a loose structure and smaller dimensions. Unlike the bare g-C_3N_4 sheets, the hierarchical structures were found in 400CN-PANI composite (Fig. 5C and D). The SEM image of 400CN-PANI composites was shown in Fig. 5C. The surface of g-C_3N_4 sheets became rough and a lot of PANI nanorods were uniformly covered on g-C_3N_4 sheets after decoration with PANI (Fig. 5D), indicating that the nucleation and growth processes only occurred on the surface of g-C_3N_4 sheets. The rough surface of 400CN-PANI was very beneficial to the propagation of visible light in the photocatalyst [35]. Moreover, this hierarchical structure allowed multiple reflections or scattering of light within the interior void, which could lead to more efficient use of the visible light.

Photocatalytic capability

The photocatalytic capabilities of g-C_3N_4 and CN-PANI composites were evaluated by comparing the degradation of MB and MO, as presented in Fig. 6. During the first 30 min illumination, only 15% of MB and 25% of MO were photodegraded by g-C_3N_4 under visible light irradiation because of the high recombination electron–hole pairs. While after modified by PANI, the photocatalytic capability of 400CN-PANI composite was significantly enhanced. The optimal photocatalytic capability of 400CN-PANI with the photodegradation efficiency was 78.6% for MB (Fig. 6A and B) and 99.8% for MO (Fig. 6C and D). When the proportion of PANI was higher, the photocatalytic capability of 600CN-PANI decreased to 67.7% for MB and 91.7% for MO. When the ratio of PANI was high, the superfluous PANI tended to aggregate on the surface of g-C_3N_4, which affected the transfer of the photo-induced carriers and separation of electron–holes pairs [36].

In the photocatalysis process, the adsorption properties of photocatalysts are of great importance. The ability of MB to get photocatalyzed may be attributed to the dye adsorption property on photocatalyst. The adsorption kinetics of the dyes on 400CN-PANI composites is shown in Fig. 7A. It was obvious that a significant adsorption could be observed in the case of MO. It can be seen from Fig. 7B that the 400CN-PANI composites possess an excellent adsorption capability for MO. It is well known that MB is a cationic dye with positively charged groups, whereas MO is an anionic dye with negatively charged groups. So there is strong electrostatic force between the negatively charged MO and positively charged sites of PANI [37,38]. In contrast, the positively charged MB cannot easily be adsorbed onto PANI due to the electrostatic repulsion.

The possible mechanism for the photocatalytic activity enhancement

It is well known that the enhancement of photocatalytic performances of the photocatalysts is mainly attributed to electrons

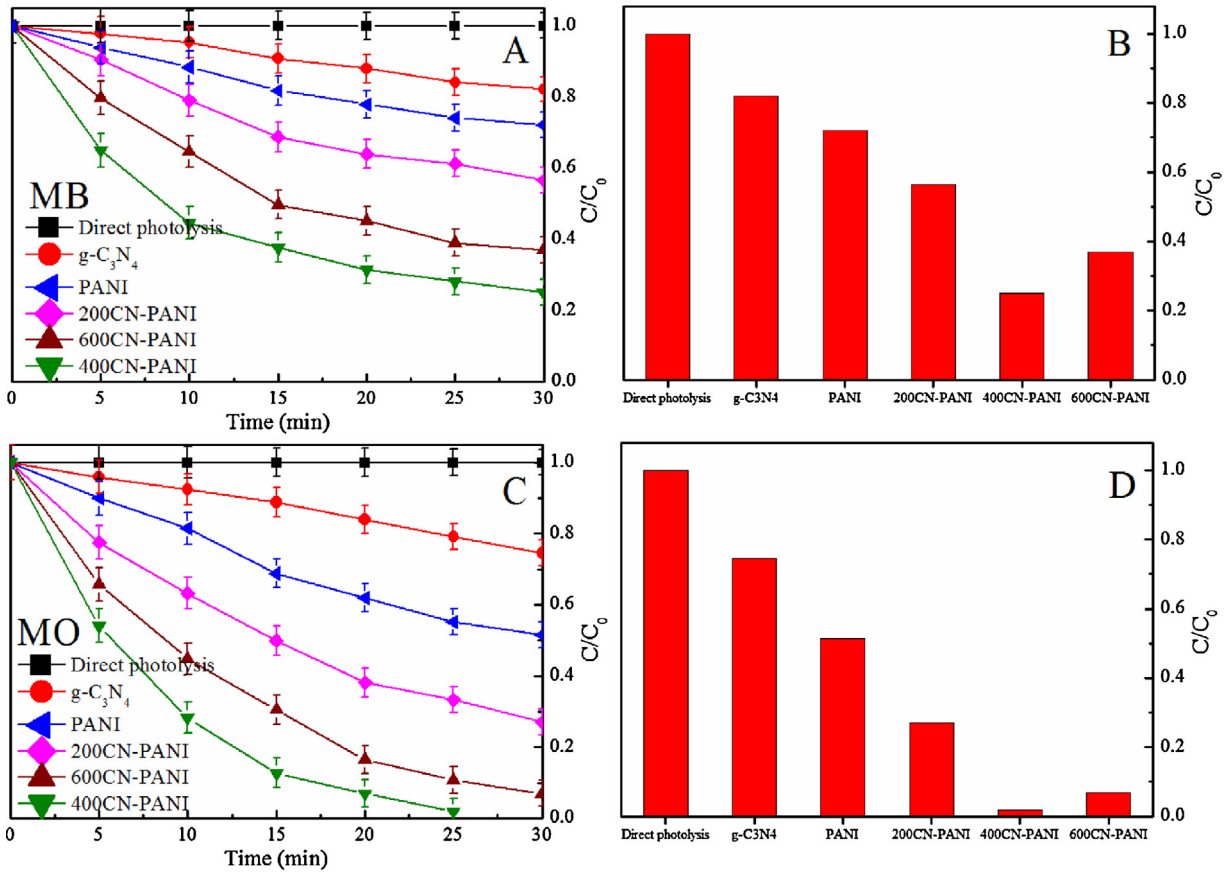

Fig. 6. Photocatalytic degradation rate of MB (A and B)/MO (C and D) under visible light irradiation in the presence of different photocatalysts.

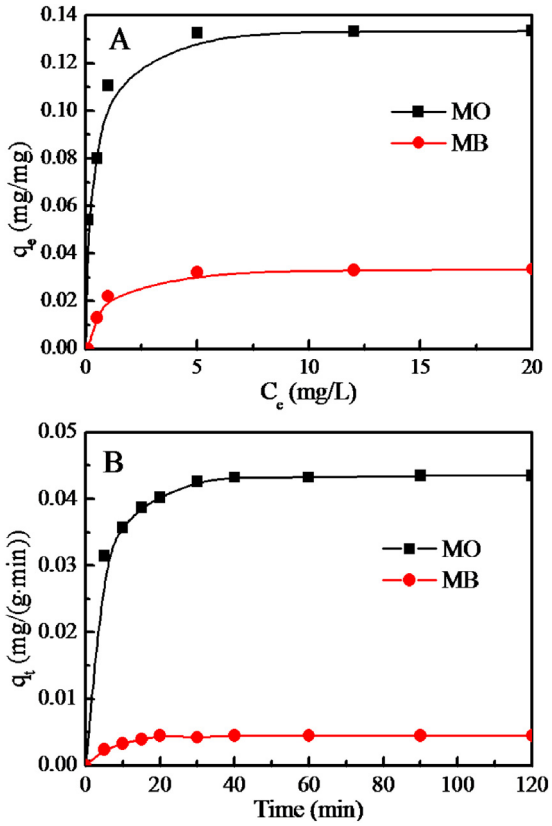

Fig. 7. Adsorption isotherms (A) and adsorption kinetics (B) of 400CN-PANI.

and holes transfer at the heterojunction interfaces [39,40]. The band gap of PANI was about ~2.77 eV using the Kubelka–Munk function, while the band gap of g-C_3N_4 is about ~2.7 eV. Therefore, when the CN-PANI composites are irradiated with visible light, both g-C_3N_4 and PANI in composites could absorb photons and excited electron–hole pairs at the same time. This process could be described as follows: the excite state electrons in PANI can readily migrate to the conduction band (CB) of g-C_3N_4. Simultaneously, the photogenerated holes in the valence band (VB) of g-C_3N_4 can directly transfer to the HOMO of PANI [41,42], which promotes the effective separation of photogenerated electron–hole pairs and decreases the probability of electron–hole pairs recombination. Meanwhile, PANI is also a good material for transporting holes [20], so the photogenerated holes can migrate easily to the surface of the photocatalyst and photodegrade the adsorbed dye molecules directly [43].

The significant enhancement in photocatalysis activity can be attributed to the remarkable synergistic effect between g-C_3N_4 and PANI [44]. As shown in Fig. 8A, the typical electrochemical impedance spectra (EIS) are presented as Nyquist plots, and it was observed that the diameter of the semicircle in the plot became shorter with the introduction of PANI, which indicated a decrease in the charge–transfer resistance on the electrode surface [45]. That is, the separation efficiency of photogenerated electrons and holes was much enhanced between g-C_3N_4 and PANI, therefore, a higher rate of photocatalysis could be achieved. Fig. 8B showed the Photoluminescence (PL) spectra of the pure g-C_3N_4 and 400CN-PANI composites excited at the wavelength of 365 nm. It could be found that the main emission peak was centered at about 456 nm for the pure g-C_3N_4, which was similar to the literature [42]. For 400CN-PANI composites, the position of the emission peak in the PL spectrum was similar to that of the pure g-C_3N_4, but the

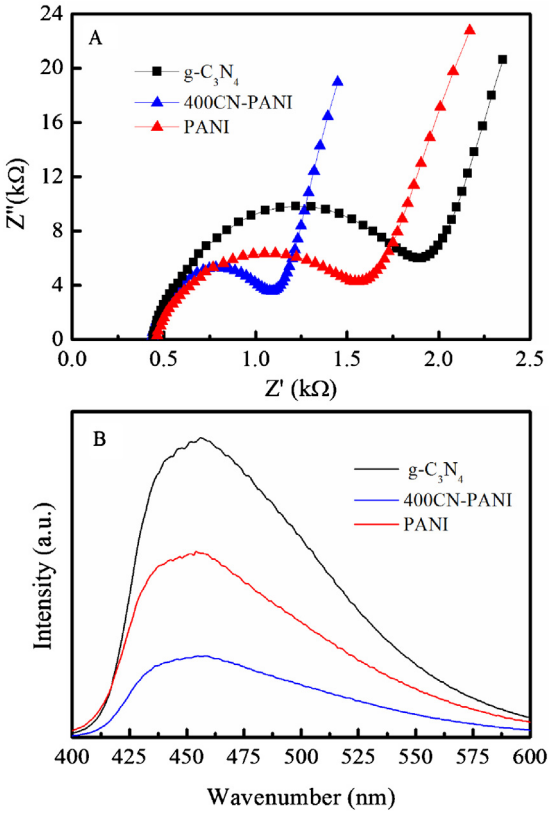

Fig. 8. (A) EIS changes of g-C_3N_4, PANI and 400CN-PANI electrodes, (B) PL spectra of g-C_3N_4, PANI and 400CN-PANI composite.

emission intensity significantly decreased, which indicated that the 400CN-PANI composites had much lower recombination rate of electron–hole pairs. That is, the recombination of photogenerated charge was greatly inhibited by the introduction of PANI, which showed that the separation efficiency of the photogenerated electron–hole pairs in 400CN-PANI composites was higher than that in pure g-C_3N_4.

It is well known that the photogenrated holes, ·OH radicals, and $\cdot O_2^-$ are three main active species in the photocatalytic process [46]. Therefore, to examine the role of these reactive species with degraded MO, a series of radicals trapping experiments were performed by using ammonium oxalate (AO), benzoquinone (BQ) and *tert*-butanol (TBA) scavengers as effective scavengers for holes, $\cdot O_2^-$ and ·OH radicals, respectively [46,47]. From the dynamic curves of MO degradation over 400CN-PANI under the visible-light in Fig. 9, we observed that the degradation rate of MO, to some extent, was suppressed by all scavengers, which indicated that holes, $\cdot O_2^-$ and ·OH radicals as oxidation sources were indeed photogenerated on the surface of composites. The possible photoreaction equations are expressed as following:

$$CN - PANI \xrightarrow{h\nu} CN(e^- \cdots h^+) - PANI(e^- \cdots h^+) \quad (1)$$

$$CN(e^- \cdots h^+) - PANI(e^- \cdots h^+) \xrightarrow{h\nu} CN \times e^- - PANI \times h^+ \quad (2)$$

$$e^- + O_2 \rightarrow \cdot O_2^- \quad (3)$$

$$\cdot O_2^- + H_2O \rightarrow \cdot OH \quad (4)$$

$$e^- + H^+ + O_2 \rightarrow H_2O_2 \quad (5)$$

$$H_2O_2 + \cdot O_2^- \rightarrow \cdot OH + OH^- + O_2 \quad (6)$$

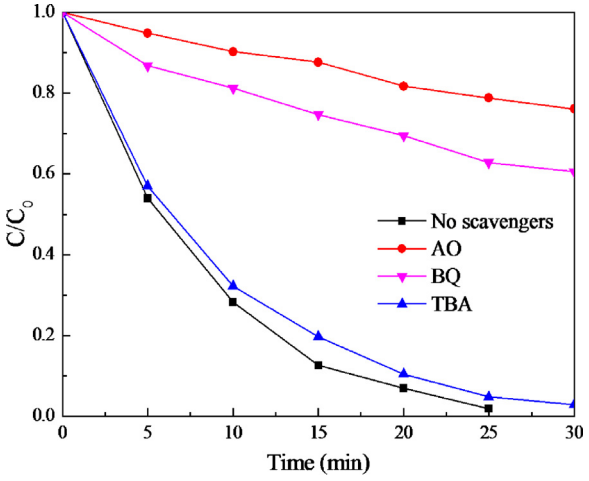

Fig. 9. (A) The effects of different scavengers on the degradation of MO in the presence of 400CN-PANI composite.

$$OH + dye \rightarrow degradation\ products \quad (7)$$

$$O_2^- + dye \rightarrow degradation\ products \quad (8)$$

$$h^+ + dye \rightarrow degradation\ products \quad (9)$$

For radicals trapping experiments (Fig. 9), without the addition of the scavengers, the photocatalytic degradation rate of MO was 99% after 30 min of visible light irradiation. After AO was added into the reaction system, the degradation rate for MO was remarkably decreased. There are following two reasons: one is that PANI as holes acceptor would produce a series of active species on its surface under visible light irradiation; the other is that the presence of high mobility of charge carriers in the circulatory system of 400CN-PANI by constantly donating electrons and accepting holes. Once the AO was added into the solution, the generation of active species and high mobility of charge carriers of the circulatory system were aborted, which seriously inhibited the photocatalytic degradation process. The BQ has the ability to trap $\cdot O_2^-$ by a simple electron transfer mechanism [47]. The addition of BQ provoked partial inhibition of the MO degradation. The results indicated that $\cdot O_2^-$ played an important role in the photocatalytic process. After TBA as a scavenger for ·OH was added in the solution, it did not obviously affect the photocatalysis activity at all. So, the photodegradation of MO was driven by the contribution of ·OH radicals to a lesser extent. To sum up, through the comparison, we can conclude that the degraded MO was mainly driven by the participation of holes and $\cdot O_2^-$ radicals, and to a lesser extent by the contribution of ·OH radicals. Therefore, the synergistic effect in the 400CN-PANI composites operated by PANI constantly donating electrons and accepting holes from g-C_3N_4, a series of active species such as holes, $\cdot O_2^-$, ·OH being successively generated in the photocatalytic process. The detailed degradation process of photocatalyst is illustrated in Scheme 1.

In addition to the special synergistic effect of both components, the excellent performance of CN-PANI composite also depends on the novel hierarchical structure of the aligned PANI nanorods. The best photocatalysis performance of such a structured material can be summarized as follows: firstly, the PANI nanorods greatly increase the specific surface area of the composites, which benefits the dye molecule diffusion from the bulky solution to the surface of the CN-PANI. Therefore, the dye molecules can easily touch the surface of the composites, leading to higher adsorption. Secondly, PANI nanorods, which have narrow diameters and thin thickness, can shorten the charge transport distance in the CN-PANI

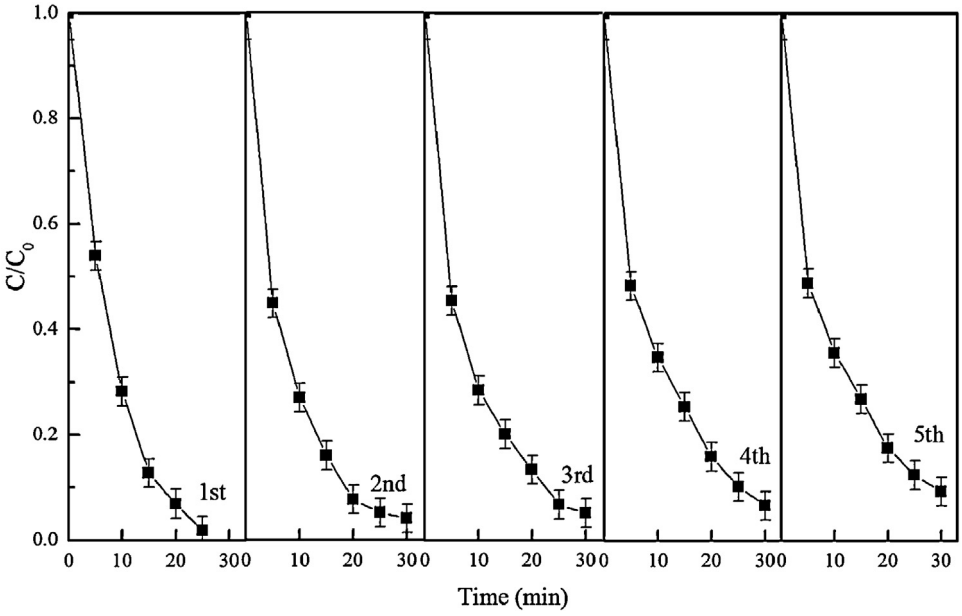

Fig. 10. Recyclability of the 400CN-PANI composite in five successive experiments for the photocatalytic degradation of MO under visible light irradiation.

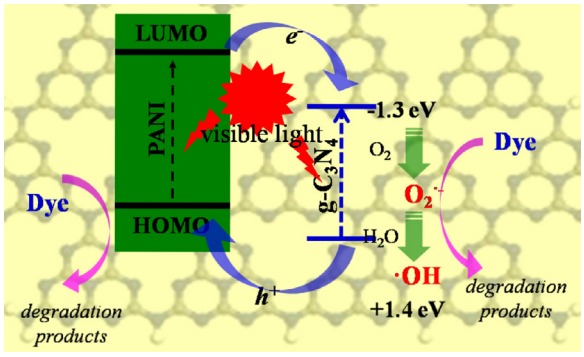

Scheme 1. Schematic diagram illustrating the mechanism of photodegradation over CN-PANI under visible light.

composite [48]. The dye molecules can easily reach the surface, realizing the efficient utilization of the photocatalyst. Narrow diameters and an optimized diffusion path can reduce diffuse resistance and the charge transfer resistance to greatly improve the photocatalysis performance [49]. Finally, due to its high conductivity as an active PANI, it can greatly reduce the photogenerated charge loss, which effectively improves the photocatalysis activity [50,51].

The stability of photocatalyst is also very important from view point of its practical application. 400CN-PANI was recycled five times in the same photocatalytic conditions. Taking into account the mass loss of photocatalyst during each reuse cycle, the former reuse cycle must be conducted twice in order to accumulate enough samples for the latter reuse cycle. Fig. 10 shows the photocatalytic performance of 400CN-PANI in the first five reuse cycles. Apparently, 400CN-PANI exhibited a certain loss of photocatalytic activity in the five reuse cycles. Therefore, CN-PANI composites could be used as high-performance and stable visible-light photocatalysts and have potential applications in environmental protection.

Conclusion

In summary, we have developed a simple and novel method for the synthesis of hierarchical CN-PANI composites by dilute polymerization. The superior visible light photocatalysis of CN-PANI can be ascribed to: (1) heterojunction being formed at the interface between g-C_3N_4 and PANI, which promotes the effective separation of photogenerated electron–hole pairs, decreasing the probability of electron–hole pairs recombination, and finally remarkably improving the visible light photocatalysis; (2) a wide and strong absorption band of PANI in the visible region making composites easy to extend photoresponse range, achieving more efficient utilization of solar spectrum; (3) good adsorption promoting the photodegradation of MO and MB. The high visible-light-driven photocatalytic activity and good stability of hierarchical CN-PANI composites render it a promising photocatalyst in efficient utilization of solar energy for the treatment of dye pollutants in environmental pollution cleanup.

Acknowledgment

This work was supported by 973 project of MOST (2011CB933700), Hefei Center for Physical Science and Technology (2012FXZY005) and National Natural Science Foundation of China (91326202, 21207136, 21272236, 21077107, 21225730).

References

[1] G.X. Zhao, L. Jiang, Y.D. He, J.X. Li, H.L. Dong, X.K. Wang, W.P. Hu, Advanced Materials 23 (2011) 3959–3963.
[2] C.C. Chen, W.H. Ma, J.C. Zhao, Chemical Society Reviews 39 (2010) 4206–4219.
[3] W. Zhao, W.H. Ma, C.C. Chen, J.C. Zhao, Z.G. Shuai, Journal of the American Chemical Society 126 (2004) 4782–4783.
[4] D.L. Zhao, G.D. Sheng, C.L. Chen, X.K. Wang, Applied Catalysis B: Environmental 111–112 (2012) 303–308.
[5] D.L. Zhao, X. Yang, C.L. Chen, X.K. Wang, Journal of Colloid and Interface Science 398 (2013) 234–239.
[6] J.C. Yu, Wi.K. Ho, J.G. Yu, H.Y. Yip, P.K. Wong, J.C. Zhao, Environmental Science and Technology 39 (2005) 1175–1179.
[7] X.C. Wang, K. Maeda, A. Thomas, K. Takanabe, G. Xin, J.M. Carlsson, K. Domen, M. Antonietti, Nature Materials 8 (2009) 76–80.
[8] L.C. Chen, D.J. Huang, S.Y. Ren, T.Q. Dong, Y.W. Chi, G.N. Chen, Nanoscale 5 (2013) 225–230.
[9] Y. Wang, X.C. Wang, M. Antonietti, Angewandte Chemie International Edition 51 (2012) 68–89.
[10] H. Xu, J. Yan, Y.G. Xu, Y.H. Song, H.M. Li, J.X. Xia, C.J. Huang, H.L. Wan, Applied Catalysis B: Environmental 129 (2013) 182–193.
[11] G. Liu, P. Niu, C. Sun, S.C. Smith, Z. Chen, G.Q. (Max) Lu, H.M. Cheng, Journal of the American Chemical Society 132 (2010) 11642–11648.
[12] S.C. Yan, Z.S. Li, Z.G. Zou, Langmuir 26 (2010) 3894–3901.

[13] Y.J. Zhang, A. Thomas, M. Antonietti, X.C. Wang, Journal of the American Chemical Society 131 (2009) 50–51.
[14] X.C. Wang, X.F. Chen, A. Thomas, X.Z. Fu, M. Antonietti, Advanced Materials 21 (2009) 1609–1612.
[15] H.J. Yan, Chemical Communication 48 (2012) 3430–3432.
[16] Q.J. Xiang, J.G. Yu, M. Jaroniec, Journal of Physical Chemistry C 115 (2011) 7355–7363.
[17] Q.J. Xiang, J.G. Yu, M. Jaroniec, Chemical Society Reviews 41 (2012) 782–796.
[18] M. Radoiičić, Z. Šaponjić, I.A. Janković, G. Ćirić-Marjanović, S.P. Ahrenkiel, M.I. Čomor, Applied Catalysis B: Environmental 136 (2013) 133–139.
[19] S.E. Shaheen, C.J. Brabec, N.S. Sariciftci, F. Padinger, T. Fromherz, J.C. Hummelen, Applied Physics Letters 78 (2001) 841–843.
[20] Y. Shirota, H. Kageyama, Chemical Reviews 107 (2007) 953–1010.
[21] H. Zhang, R.L. Zong, Y.F. Zhu, Journal of Physical Chemistry C 113 (2009) 4605–4611.
[22] F. Wang, S.X. Min, Chinese Chemical Letters 18 (2007) 1273–1277.
[23] H. Zhang, Y.F. Zhu, Journal of Physical Chemistry C 114 (2010) 5822–5826.
[24] M. Shang, W.Z. Wang, S.M. Sun, J. Ren, L. Zhou, L. Zhang, Journal of Physical Chemistry C 113 (2009) 20228–20233.
[25] Y.B. Wang, J.D. Hong, W. Zhang, R. Xu, Catalysis Science and Technology 3 (2013) 1703–1711.
[26] N.R. Chiou, C.M. Lui, J.J. Guan, L.J. Lee, A.J. Epstein, Nature Nanotechnology 2 (2007) 354–357.
[27] X.C. Wang, K. Maeda, X.F. Chen, K. Takanabe, K. Domen, Y.D. Hou, X.Z. Fu, M. Antonietti, Journal of the American Chemical Society 131 (2009) 1680–1681.
[28] Y.S. Yang, M.X. Wan, Journal of Materials Chemistry 12 (2002) 897–901.
[29] J.D. Hong, X.Y. Xia, Y.S. Wang, R. Xu, Journal of Materials Chemistry 22 (2012) 15006–15012.
[30] S.W. Zhang, M.Y. Zeng, W.Q. Xu, J.X. Li, J. Li, J.Z. Xu, X.K. Wang, Dalton Transactions 42 (2013) 7854–7858.
[31] Y. Chen, J.S. Zhang, M.W. Zhang, X.C. Wang, Chemical Science 4 (2013) 3244–3248.
[32] X.F. Wang, Y.H. Shen, A.J. Xie, L.G. Qiu, S.K. Li, Y. Wang, Journal of Materials Chemistry 21 (2011) 9641–9646.
[33] J. Li, L.H. Zhu, Y.H. Wu, Y. Harima, A.Q. Zhang, H.Q. Tang, Polymer 47 (2006) 7361–7367.
[34] J.Y. Luo, H.D. Jang, T. Sun, L. Xiao, Z. He, A.P. Katsoulidis, M.G. Kanatzidis, J.M. Gibson, J.X. Huang, ACS Nano 5 (2011) 8943–8949.
[35] X.C. Wang, J.C. Yu, C.M. Ho, Y.D. Hou, X.Z. Fu, Langmuir 21 (2005) 2552–2559.
[36] H. Zhang, R.L. Zong, J.C. Zhao, Y.F. Zhu, Environmental Science and Technology 42 (2008) 3803–3807.
[37] D. Mahanta, G. Madras, S. Radhakrishnan, S. Patil, Journal of Physical Chemistry B 112 (2008) 10153–10157.
[38] D. Mahanta, G. Madras, S. Radhakrishnan, S. Patil, Journal of Physical Chemistry B 113 (2009) 2293–2299.
[39] J.S. Zhang, M.W. Zhang, R.Q. Sun, X.C. Wang, Angewandte Chemie International Edition 51 (2012) 10145–10149.
[40] S.W. Zhang, J.X. Li, H.H. Niu, W.Q. Xu, J.Z. Xu, W.P. Hu, X.K. Wang, ChemPlusChem 78 (2013) 192–199.
[41] W.H. Leng, Z. Zhang, J.Q. Zhang, C.N. Cao, Journal of Physical Chemistry B 109 (2005) 15008–15023.
[42] S.B. Yang, Y.J. Gong, J.S. Zhang, L. Zhan, L.L. Ma, Z.Y. Fang, R. Vajtai, X.C. Wang, P.M. Ajayan, Advanced Materials 25 (2013) 2452–2456.
[43] E.R. Carrway, A.J. Hoffman, M.R. Hoffmann, Environmental Science and Technology 28 (1994) 776–785.
[44] X.Y. Li, D.S. Wang, G.X. Cheng, Q.Z. Luo, J. An, Y.H. Wang, Applied Catalysis B: Environmental 81 (2008) 267–273.
[45] X.M. Tu, S.L. Luo, G.X. Chen, J.H. Li, Chemistry—A European Journal 18 (2012) 14359–14366.
[46] A.A. Khodja, T. Sehili, J.F. Pilichowski, P. Boule, Journal of Photochemistry and Photobiology A: Chemistry 14 (2001) 231–239.
[47] E. Baciocchi, T.D. Giacco, F. Elisei, M.F. Gerini, M. Guerra, A. Lapi, P. Liberali, Journal of the American Chemical Society 125 (2003) 16444–16454.
[48] H. Zhang, G.P. Cao, W.K. Wang, K.G. Yuan, B. Xu, W.F. Zhang, J. Cheng, Y.S. Yang, Electrochimica Acta 54 (2009) 1153–1159.
[49] L. Cao, F. Xu, Y.Y. Liang, H.L. Li, Advanced Materials 16 (2004) 1853–1857.
[50] Y.G. Wang, H.Q. Li, Y.Y. Xia, Advanced Materials 18 (2006) 2619–2623.
[51] Q. Wang, X.K. Wang, Z.F. Chai, W.P. Hu, Chemical Society Review 40 (2013) 8821–8834.